Dynamic Analysis of Gyroscopic Force Redistribution for a Wheeled Rover

C. A. Cao[1]; D. K. Lieu[2]; and H. S. Stuart[3]

[1]Univ. of California, Berkeley (corresponding author). Email: cyndia_cao@berkeley.edu
[2]Univ. of California, Berkeley
[3]Univ. of California, Berkeley

ABSTRACT

Current Mars rovers feature large, complex suspensions to overcome obstacles. Unfavorable contact force distribution can cause slip and high drive torque demands. When traversing step-like obstacles, the vehicle is most likely to slip when the back wheels start trying to ascend the obstacle. Minimizing the ratio of tractive force to normal force on each wheel is one traction control strategy to reduce slip. This work analyzes the potential integration of a control moment gyroscope on a four-wheel rover to induce pitch moments on the rover and more effectively distribute contact loads, such that slip is avoided and drive torque requirements are reduced. For the baseline 400 kg rover considered with 0.5 m diameter wheels ascending a 0.35 m step, maximum drive torque was reduced by 40%, and maximum tractive to normal force ratio was reduced by 70%, with a total mean power comparable to normal driving. While there are mechanical challenges associated with implementing control moment gyroscopes, this analysis motivates further theoretical and experimental work in the evaluation of gyroscopic force redistribution for improving rover mobility.

BACKGROUND

Despite a growing history of planetary rover deployment, many terrains remain difficult to impossible to navigate and continue motivating development of new locomotion systems. The Mars 2020 rover is expected to encounter long, unavoidable fractures in bedrock, which will require the ability to climb step-like obstacles. Current Mars rovers feature six wheels and large complex suspensions to overcome obstacles. However, unfavorable internal force distribution when the back wheels begin to ascend causes slip and high drive torque demands that limit mobility.

The rocker bogie passive suspension is the current standard for rover design, but researchers have proposed more configurations with varying degrees of active control to tackle existing mobility challenges (Cordes et al. 2018; Fauroux et al. 2006; Schenker et al. 2000; Thueer et al. 2006; Wettergreen et al. 2010). These solutions use a combination of passive kinematics and active manipulation of wheel pose to improve the distribution of mass over their wheels. While active suspensions have increased mass distribution control, they also require more complicated kinematic control. Since the mass of the vehicle is concentrated at the center, significant force redistribution would require large suspension travel. A mode of contact force redistribution that has not yet been explored for wheeled locomotion is gyroscopic torque, which can be generated at large magnitudes for short periods and would be dynamically appropriate for step obstacle traversal.

A gyroscope is a flywheel that is gimbaled such that the angular momentum vector direction can be reoriented, or precessed. Upon precession, conservation of angular momentum causes a gyroscopic torque about a vector orthogonal to the spin and precession axes. The three standard

gyroscope configurations are a single gimbal degree of freedom (DOF) gyroscope, a double gimbal gyroscope with two orthogonal control axes, and two single DOF gyroscopes that are spun and precessed in opposing directions. A single DOF gyroscope can create gyroscopic torques orders of magnitude greater than the input precession torque.

Control Moment Gyroscopes (CMG) are particularly useful in space applications where gravity is low and there are no surfaces available to react loads against, so disturbances must be counteracted internally. CMG's are a standard method for attitude control of satellites, including the International Space Station (Gurrisi et al. 2010). Anti-precessed CMG pairs, also called counter-rotating pairs or a twin gyro, were also studied for the control of robotic arms in space because they can control end effectors with torques that are decoupled from the rest of the robot body (Brown 2008). A cube-shaped robot called Hedgehog was designed to travel the surface of an asteroid using three orthogonal reaction wheels to roll the cube in the desired direction of motion (Hockman et al. 2017). This torque can be employed effectively in low gravity (e.g. Mars or the moon) since the magnitude of its output is significant relative to gravitational forces.

DYNAMIC MODEL

A simplified static analysis of a four-wheel chassis driving over a step, as in Figure 1, highlights the primary challenge of lifting the rear wheel. When the front wheels ascend, the load concentrates on the back wheels. Assuming an arbitrary tractive force can be applied, the back wheels need to apply high forces to counteract the concentrated load. However, a metal wheel on smooth rock can typically only apply a tractive force that is up to ~40% of its normal load before slipping. Tractive force can be applied at the front wheel to generate normal load on the back wheel, but as the obstacle gets much taller than a wheel radius, it becomes impossible to reduce the tractive force to normal force ratio to a level with no slip. If there are asperities in the surface that can mechanically support the load by interlocking with the wheel treads, then a wheel can apply increased tractive force, but large drive torques are required.

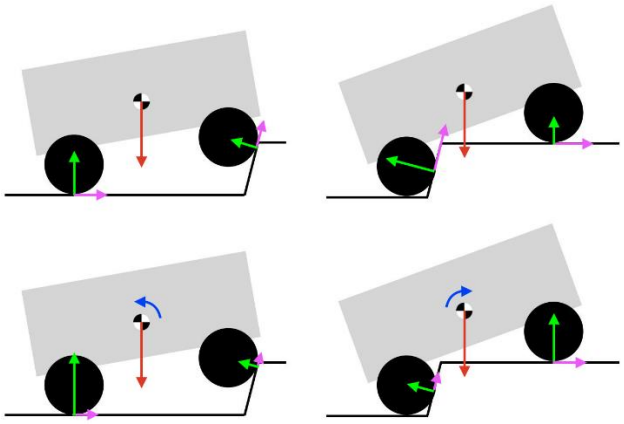

Figure 1. Illustration of the forces acting on the rover. During typical driving (top), the normal force at each wheel depends on the location of the center of mass relative to each wheel. An additional body torque (bottom, shown in blue) causes normal forces to redistribute.

Traction control strategies often use torque control to minimize tractive force to normal force ratio for each wheel, physically maximizing the margin to wheel slip on arbitrary surfaces (Iagnemma and Dubowsky 2004; Krebs et al. 2010; Siravuru et al. 2017). These previous works focus on passive chassis and use each wheel's drive torque as the primary inputs. We propose using internal gyroscopic torque as an additional control input for further optimization.

To explore the dynamics of gyroscopic force redistribution, a rover is assumed to have four rigidly attached wheels and to be moving slowly enough to be considered a quasi-static problem. In a simplified 2D step-climbing context, this model could represent a driving mode of any of the four-wheel suspensions currently employed by NASA, including test rover Scarab and future lunar rover VIPER.

The tractive to normal force ratio of each wheel is minimized over the entire step traversal trajectory to estimate optimal drive torque and gyroscopic torque inputs. The rover's kinematics were calculated at discrete points along its entire trajectory to create force and moment balance constraints at every location. Mathematically, the control optimization takes the following form, where the arguments are the drive torques of each wheel and the gyroscopically applied redistribution torque at every point in time.

$$\min \sum_{t}^{T} \left(\left(\sum_{i}^{n} \left(c_{FR} \frac{T_i}{N_i} \right)^2 \right) + \left(\frac{1}{c_g} \tau_{gyro} \right)^2 \right)$$

$$\begin{aligned} \text{s.t. at every } t, \Sigma F_x &= 0 \\ \Sigma F_z &= 0 \\ \Sigma M &= 0 \end{aligned}$$

where T_i and N_i are the tractive force and normal force applied by the i^{th} wheel at the surface contact point, n is the number of wheels, and c_{FR} and c_g are cost scaling variables to tune the weight of a high force ratio and a high gyroscopic torque application, respectively.

For dynamic simplicity, a twin gyro configuration was chosen. This gyro has two flywheels spinning in opposite directions such that their angular momentums sum to zero when their axes are aligned. They are gimbaled by equal and opposite angles to produce a change of angular momentum which is confined to a single vector direction, i.e. the pitch direction in this case, whereas a lone single-DOF gyro would produce a gyroscopic torque vector whose direction follows the changing gimbal position. Furthermore, the counter-balanced nature of the angular momentum in this system results in output torque insensitivity to external vehicle rates.

Since the goal is to produce torque about the pitch axis, we constrain the flywheel with spin axis in the vertical (vehicle yaw) direction and gimbal axis in the forward (vehicle roll) direction. Without considering vehicle rotation, the gyroscopic torque output by one flywheel is

$$\boldsymbol{\tau} = I_a \boldsymbol{\omega} \times \dot{\boldsymbol{\phi}} = I_a \omega \dot{\phi} \left(\cos\phi \, \hat{\boldsymbol{j}} + \sin\phi \, \hat{\boldsymbol{k}} \right)$$
$$\tau_{gimbal} = I_t \ddot{\phi}$$

where $\boldsymbol{\omega}$ represents the vector spin rate in the direction of the spin axis, $\dot{\boldsymbol{\phi}}$ represents the vector gimbal rate in the direction of the gimbal axis, and $\boldsymbol{\tau}$ is the resulting gyroscopic torque. I_a is the axial moment of inertia of the flywheel, and I_t is the moment of inertia of the gimballed system, approximated now as the transverse moment of inertia of the flywheel. Finally, τ_{gimbal}

is the torque required to actuate the gimbal. Note that a similar result can be obtained from a flywheel with its spin axis forward and gimbal axis vertical.

A twin gyro composed of two counter-rotating, counter-precessed single-DOF gyros as described above would instead be characterized as

$$\boldsymbol{\tau} = 2I_a\omega\dot{\phi}\cos\phi\,\hat{\boldsymbol{j}}$$
$$\tau_{gimbal} = 2I_t\ddot{\phi} + (2I_a\omega\cos\phi)\,q$$

where vehicle rates are now considered, and q is the pitch rate (Jacot and Liska 1966). The external pitch motion causes a torque on each flywheel which is orthogonal to the spin axis, a portion of which must be sustained by the actuation axis.

An example of an optimized step-climbing event, using the mechanical and optimization parameters listed in Table 1 and seen in Figure 2, shows how normal force concentrates on the wheel that is on the flat surface, where it can more effectively produce forward force. Normal force is shifted away from the inclined surface, which resists forward motion. Compared to a rover with no gyroscopic torque control (dashed lines), the gyro reduces the maximum force ratio from 1.6 to 0.5, which is a more achievable value. The drive torque is also reduced from a maximum of 113 N-m and 166 N-m for the front and back wheels, respectively, to about 100 N-m for both. The optimization is independent of gyroscope design and rover velocity.

Table 1. Mechanical system and optimization parameters.

Rover	Gyroscope	Optimization Parameters
• Mass: 400 kg	• Outer diameter: 0.35 m	• c_{FR}: 5
• Wheel diameter: 0.5 m	• Inner diameter: 0.2 m	• c_g: 240
• Wheelbase: 1.2 m	• Height: 0.05 m	
• COM height: 0.6 m	• Density: steel (~8000 kg/m^3)	
• Velocity: 10 cm/s	• Spin rate: 15,000 rpm	
• Gravity: 3.71 m/s^2	• Angular momentum: 827 kg-m^2/s	

Figure 3 shows the gimbal trajectory required to produce the desired gyroscopic torque, which is defined by the flywheel's angular momentum. The actuation torque depends on not only the angular momentum but also the pitch rate of the rover. As pitch rate is reduced by driving more slowly, the gyroscope must generate torque for a longer time, which is ultimately limited by saturation when the gimbal approaches 90°. Similarly reducing flywheel size and speed to reduce actuation torque would require faster gimbaling and larger angular sweeps. Larger obstacles also require increased gimbaling, so the parameters of a gyroscope must be designed with a specific use case.

Figure 4 shows the cumulative power requirement of each motor at every time step. The total power required by a standard rover is shown by the dashed purple line and is dominated by the rear wheel as it ascends the step. The total power required by the rover with a gyroscope is shown by the solid grey line. The gimbal motor draws the most power but significantly reduces the maximum power requirement of both drive motors. Over the full simulation period, the average power draw is about the same. No power optimization was done thus far but could be a part of future work. Furthermore, the results assume a successful climb; however, we would expect that the rover without the gyro would spend more time struggling with slip or lack of sufficient torque, which would align with high power consumption events.

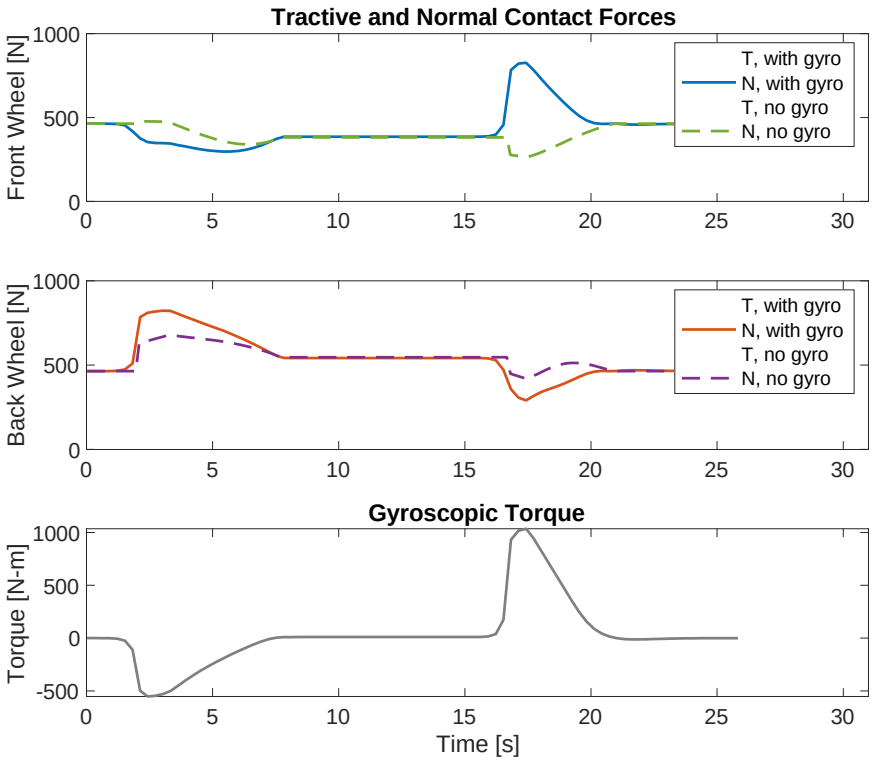

Figure 2. A sample optimal drive traction and gyroscopic torque input trajectory for a rover climbing a 0.35m step. A negative gyroscopic torque is applied to lift the front wheel over the step and a positive torque to lift the back wheel. The step is 40% taller than the wheel radius and would be extremely challenging for a traditional rover, represented by the dashed lines.

Trends for this rover as it ascends steps of varying heights are shown in Figure 5. The maximum force ratio and torque inputs occur either when the front wheels or back wheels first contact the step. Once the step is greater than wheel radius in height, the initial contact kinematics are roughly the same regardless of step height, thus the trends flatten for steps greater than 0.25 m. The first 2 plots apply regardless of gyro size and rover velocity, while the gyro actuation torque and power vary. The balance between maximum force ratio and applied gyroscopic torque is controlled by their relative cost scales c_{FR} and c_g. The effect of c_g is shown in Figure 6. If surface conditions improve, such as by technology development in tire traction, then c_g can be decreased to increase the force ratio and decrease the applied gyroscopic torque.

DISCUSSION

Gyroscopic redistribution of forces can provide dynamic benefits to rover locomotion over obstacles. While a single rover configuration was considered, further design space analysis can be performed with varying rover size and mass, rover speed, wheel diameter, and obstacle height in order to understand their effects on locomotion and the application of gyroscopic torque. The concept is most applicable to large rovers since flywheel moment of inertia increases quartically with radius. It is also compelling for lightweight rovers or rovers operating in particularly low gravity, such as on the moon.

Gyroscope design depends on the desired torque output, for which magnitude and duration are limited by saturation. In order to produce greater or extended torques, a gyroscope must gimbal faster or over a longer range of angles, respectively. If close to saturation, the flywheel's angular momentum must be increased, which increases the required gimbal holding torque during pitching. Further analysis will include optimization of gimbal power, which is influenced by gimbal position and vehicle velocity (currently held constant) in order to improve its implementation.

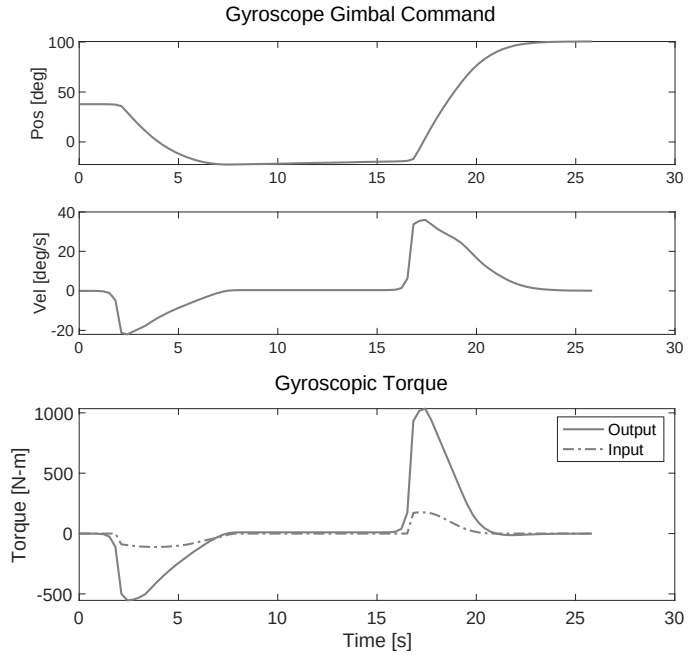

Figure 3. Gimbal trajectory and output for specified flywheel. Note that a majority of the gimbal actuation torque is required in reaction to the pitch rate of the rover.

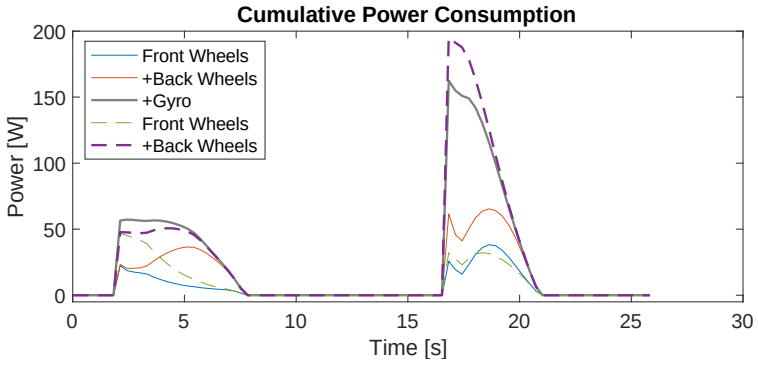

Figure 4. Cumulative power contributions of the drive and gimbal motors. Without optimizing power consumption of the gyroscope, the two systems have a similar mean power requirement (17.4 W vs. 18.2 W with and without a gyro, respectively).

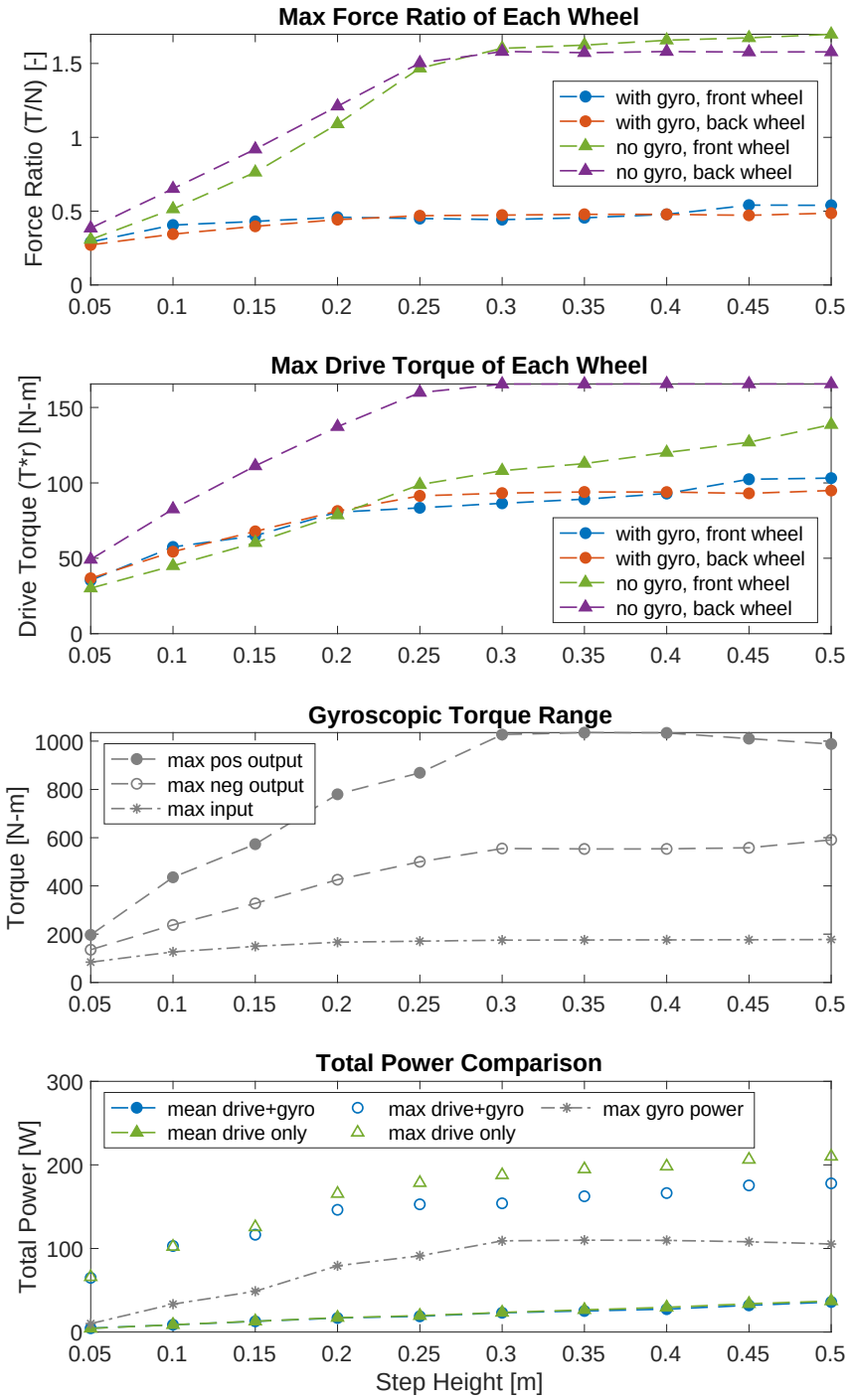

Figure 5. Maximum force ratio and drive torque as step height increases. The challenge increases with step height until it reaches wheel diameter due to less favorable initial wheel contact angles. Afterwards, every step height has roughly the same worst case impact on locomotion.

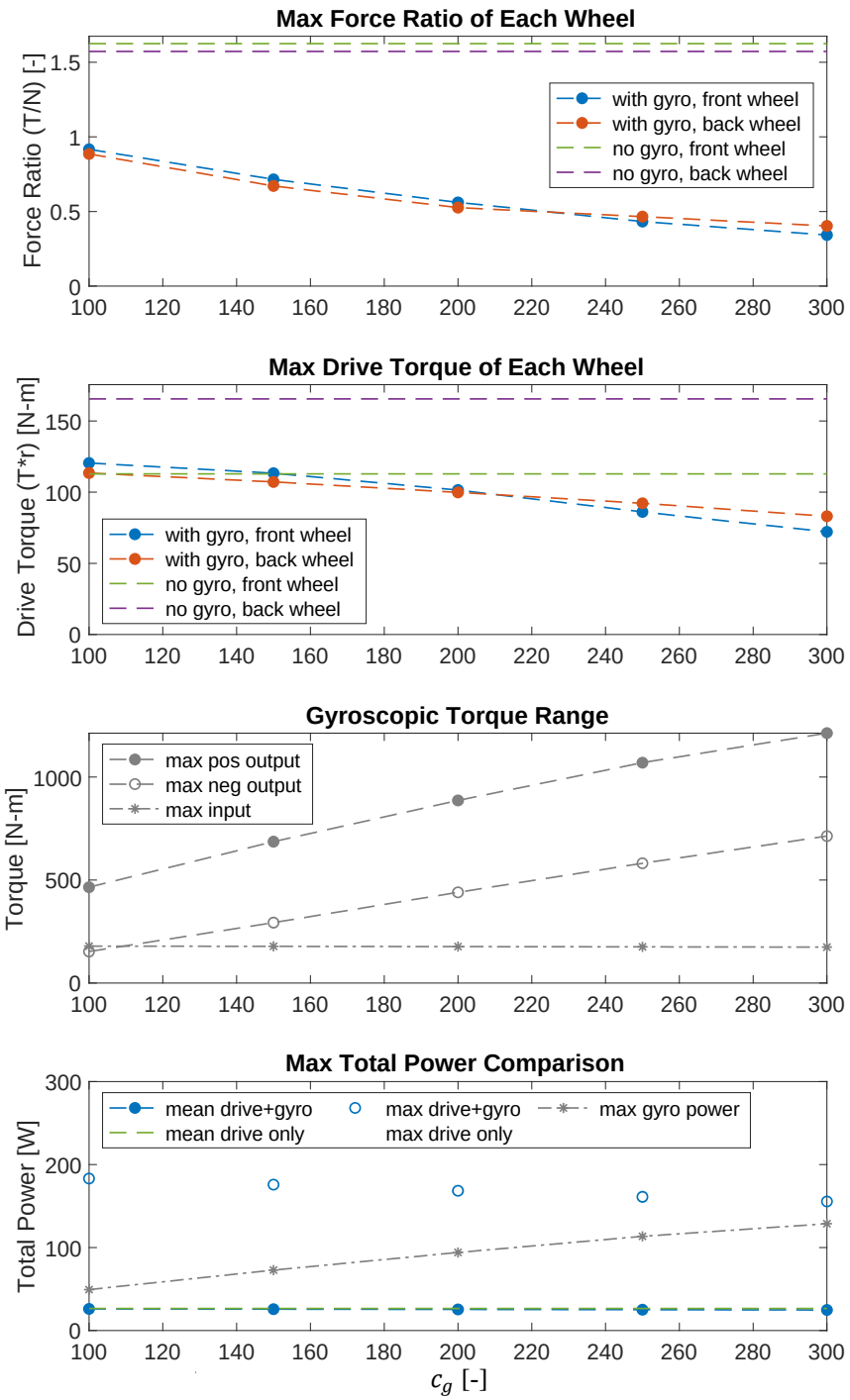

Figure 6. Maximum force ratio and drive torque with varying relative optimization costs. As the cost of applying torque decreases (c_g increases), the maximum force ratio and drive torque decrease. The gimbal input torque is insensitive to applied gyroscopic torque, since it primarily must counteract the vehicle pitch rate. However, gimbal power increases due to faster gimbal rates.

This work presents a method for analyzing potential for mobility improvement via gyroscopic torque control, specific to ascending large, step-like obstacles. However, it addresses traction conservatively by minimizing contact force ratio, thus providing the best possible safety factor to prevent slip. Real surfaces are often not smooth and slippery, but rather have rough rocky features that improve traction and thus reduce the magnitude of gyroscopic actuation that is necessary. The limiting factor may instead be the drive motor's maximum torque. Thus, the optimization cost function can be changed according to need.

CONCLUSION

Gyroscopic force redistribution can reduce wheel slip, reduce drive motor torque requirements, and increase the region of traversable terrain of a future Mars mission. Specifically, this may be compelling for a mission like Mars Sample Return, during which a rover is expected to quickly retrieve the samples obtained by the Mars 2020 rover. This could enable a smaller rover than the flagship rocker-bogie solution, which requires 6 wheels and a large suspension system.

While a number of works previously introduce the concept of shifting mass using active suspensions, force and speed. Scales are small compared with the proposed gyroscopic solution. We therefore expect that gyros can uniquely influence highly dynamic maneuvering over larger obstacles. However, these technologies are not mutually exclusive, and any combination must factor in both gyroscopic torque transferability and nominal kinematic stability.

This work is part of a series of investigations to understand scenarios in which dynamic contact force shifting could improve wheeled rover mobility. A gyroscope is a precision mechanical system; flywheel balance and gimbal alignment are critical, so its value must be weighed against complexity and cost for each specific use case. This work is theoretical so far, and experimental execution will be necessary to determine practical challenges and feasibility.

ACKNOWLEDGEMENTS

This work was supported by a NASA Space & Technology Fellowship, grant number 80NSSC19K1167 Mobility Evaluation of a Planetary Rover with Gyroscopic Force Redistribution Control, in collaboration with Colin Creager at the NASA Glenn Research Center.

REFERENCES

Brown, D. (2008). "*Control moment Gyros as space-robotics actuators.*" American Institute of Aeronautics and Astronautics, Honolulu, Hawaii.

Cordes, F., Kirchner, F., and Babu, A. (2018). "Design and field testing of a rover with an actively articulated suspension system in a Mars analog terrain." *Journal of Field Robotics*, 35(7), 1149–1181.

Fauroux, J. C., Chapelle, F., and Bouzgarrou, B. C. (2006). "A new principle for climbing wheeled robots: Serpentine climbing with the open wheel platform." 2006 *IEEE/RSJ International Conference on Intelligent Robots and Systems*, IEEE, Beijing, China.

Gurrisi, C., Seidel, R., Dickerson, S., Didziulis, S., Frantz, P., and Ferguson, K. (2010). "Space station control moment gyroscope lessons learned." *Proceedings of the 40th Aerospace Mechanisms Symposium*, Cocoa Beach, FL, 16.

Hockman, B. J., Frick, A., Reid, R. G., Nesnas, I. A. D., and Pavone, M. (2017). "Design, control, and experimentation of internally-actuated rovers for the exploration of low-gravity planetary bodies." *Journal of Field Robotics*, 34(1), 5–24.

Iagnemma, K., and Dubowsky, S. (2004). "Traction control of wheeled robotic vehicles in rough Terrain with application to planetary rovers." *The International Journal of Robotics Research*, 23(10–11), 1029–1040.

Jacot, A. D., and Liska, D. J. (1966). "Control moment gyros in attitude control." *Journal of Spacecraft and Rockets*, 3(9), 1313–1320.

Krebs, A., Risch, F., Thueer, T., Maye, J., Pradalier, C., and Siegwart, R. (2010). "Rover control based on an optimal torque distribution - Application to 6 motorized wheels passive rover." 2010 *IEEE/RSJ International Conference on Intelligent Robots and Systems*, IEEE, Taipei.

Schenker, P. S., Pirjanian, P., Balaram, J., Ali, K. S., Trebi-Ollennu, A., Huntsberger, T. L., Aghazarian, H., Kennedy, B. A., Baumgartner, E. T., Iagnemma, K. D., Rzepniewski, A., Dubowsky, S., Leger, P. C., Apostolopoulos, D., and McKee, G. T. (2000). "Reconfigurable robots for all-terrain exploration." *Sensor fusion and decentralized control in robotic systems III*, International Society for Optics and Photonics, Boston, MA, 454–468.

Siravuru, A., Shah, S. V., and Krishna, K. M. (2017). "An optimal wheel-torque control on a compliant modular robot for wheel-slip minimization." *Robotica*, 35(2), 463–482.

Thueer, T., Lamon, P., Krebs, A., and Siegwart, R. (2006). "CRAB – Exploration rover with advanced obstacle negotiation capabilities." 9th *ESA Workshop on Advanced Space Technologies for Robotics and Automation*, Noordwijk, The Netherlands.

Toupet, O., Biesiadecki, J., Rankin, A., Steffy, A., Meirion-Griffith, G., Levine, D., Schadegg, M., and Maimone, M. (2018). "Traction control design and integration onboard the Mars science laboratory curiosity rover." 2018 *IEEE Aerospace Conference*, IEEE, Big Sky, MT.

Wettergreen, D., Moreland, S., Skonieczny, K., Jonak, D., Kohanbash, D., and Teza, J. (2010). "Design and field experimentation of a prototype Lunar prospector." *The International Journal of Robotics Research*, 29(12), 1550–1564.